IEEE Access
Multidisciplinary | Rapid Review | Open Access Journal

Received 12 August 2022, accepted 16 September 2022, date of publication 26 September 2022, date of current version 4 October 2022.

Digital Object Identifier 10.1109/ACCESS.2022.3209650

RESEARCH ARTICLE

An Adaptive Emergency Approach for Hybrid Networked Microgrids Resilience

AYDA SHAKER[1,2], (Student Member, IEEE), MOKHTAR BOZORG[2], (Member, IEEE), AMIN SAFARI[1], AND SAJAD NAJAFI-RAVADANEGH[1], (Member, IEEE)

[1]Department of Electrical Engineering, Azarbaijan Shahid Madani University, Tabriz 53714-161, Iran
[2]School of Management and Engineering Vaud (HEIG-VD), University of Applied Sciences and Arts of Western Switzerland (HES-SO), 2800 Yverdon-les-Bains, Switzerland

Corresponding author: Ayda Shaker (ayda.shaker@heig-vd.ch)

ABSTRACT The low inertia of renewable-based distributed energy resources (DERs) renders hybrid networked microgrids (NμGs) dynamically susceptible to transients. Such fragility makes it very difficult for NμGs operators to maintain a reasonable margin for the resilient operation during extreme condition contingencies. This paper presents a three-stage emergency approach to improve resilience of NμGs through maintaining dynamic security. The proposed approach targets preserving the resilient operation of NμGs by preventing unnecessary tripping of the DERs after unintentional islanding incident. To do so, a resilient operation zone (ROZ) is introduced which determines the secure operating zone for NμGs and the limits for implementing the corrective countermeasures for resilience augmentation. The proposed approach is outlined in three stages: First, offline analysis is carried out to model and calculate the ROZ. Second, hybrid NμGs operating point is monitored at the pre-event stage and the calculated ROZ at offline stage is adapted to the operating conditions. The third stage is responsible for real-time evaluation of hybrid NμGs security using the ROZ and implementation of the countermeasures. Comprehensive simulation studies presented in this paper demonstrate effectiveness of the proposed scheme for enhancing resilience of hybrid NμGs.

INDEX TERMS Hybrid AC/DC microgrids, resilient power systems, emergency approach.

I. INTRODUCTION

A. BACKGROUND

In recent years, extreme weather-related and man-made events have led to more intense and frequent interruptions in normal operation of conventional power systems [1]. Tremendous socio-economic consequences of such extreme events have promoted the concept of power system resilience [2]. To establish a resilient power system, the conventional notion of bulk power system utilization has been revisited as the concept of distributed operation, say microgrids (μGs) [3].

Deployment of grid-connected AC μGs with specific objectives, say hospitals, refineries, and alike, is a common practice for power system resilience. By proliferation of renewable-based distributed energy resources (DERs) and DC loads, DC μGs are also became attractive [4]. Although individual AC and DC μGs may enhance the resilience of the entire power system, the power system resilience could be further improved by networking the adjacent individual μGs and establishing networked μGs (NμGs) [5]. A NμG might include only AC or DC μGs; however, AC and DC μGs can be practically networked to configure hybrid AC/DC NμGs which can contribute more to the power system resilience.

The associate editor coordinating the review of this manuscript and approving it for publication was Maurizio Casoni.

B. LITERATURE REVIEW

During extreme condition contingencies, when the upstream power supply is interrupted [6], the NμGs are exposed to an unintentional islanding incident which can challenge the resilient operation of the NμGs. The main reason is the low physical inertia of power-electronic converters which render hybrid NμGs dynamically fragile against incipient transients and makes it very difficult for NμGs operators to maintain a reasonable margin for the resilient operation [7]. Due to such a vulnerability, certain procedures and grid codes have recommended fast DER tripping through the loss of mains

protection (ANSI Code 78) upon an unintentional islanding event [8], [9]. Although DER tripping during extreme events might rescue the low-inertia DERs from likely damages, it would significantly degrade the resilient operation of hybrid NμGs. The degraded NμGs and tripped DERs might be restored through black-start mechanisms; however, this might be a very difficult task, particularly under severe weather conditions [10]. To cope with this issue and to establish a resilient operation: 1) The immediate tripping of DERs should be suspended; 2) The DERs should remain in service to the boundaries of dynamic insecurity [11]; and, 3) Proper emergency countermeasures should be adopted to preserve the dynamic security, and in consequence, promote the resilient operation of the NμGs. In this regard, out-of-step protection schemes are offered to distinguish the borders of dynamic security [12]. Hence, the DERs can remain in-service subsequent to an unintentional islanding event until the trip signal is issued by out-of-step protection. However, out-of-step relays are mostly applied to bulk power systems with considerable inertia and are deemed inefficient for low-inertia μGs [13]. In [14], undervoltage relay is offered to detect the dynamic security boundaries. However, the lack of selectivity in voltage-based protection schemes can also lead to unnecessary tripping of DERs. A new scheme based on the operation concept of existing overcurrent and undervoltage relays is offered in [15] to detect the borders of dynamic security. The method proposed in [15] considers the normal contingencies such as short-circuit events rather than extreme condition contingences, say unintentional islanding.

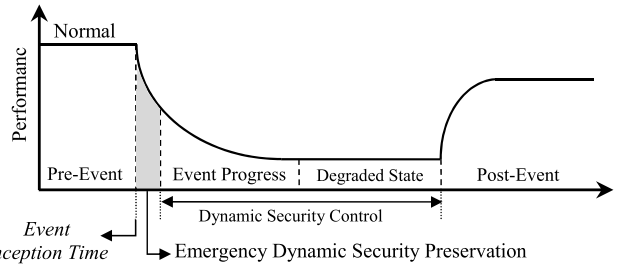

FIGURE 1. Performance of a power system subsequent to an extreme event.

Most of the available researches in the literature for preserving the dynamic security, and in consequence, boosting up the resilience of NμGs, are control-oriented solutions [16], [17], [18], [19], [20], [21]. Although being effective to govern the dynamic security, such control approaches are usually triggered after dynamic security preservation stage. To offer more details, the performance of a power system while facing an extreme event is depicted in Fig. 1. In Fig. 1, the emergency dynamic security preservation stage is a very narrow range within which, the emergency countermeasures should be applied. However, the control mechanisms offered by [16], [17], [18], [19], [20], and [21] occurs afterwards, at the event progress and degraded stages, when the dynamic insecurity might already has happened.

C. RESEARCH GAPS AND CONTRIBUTIONS

Based on the literature review study presented in Section I.A, it can be observed that resilience enhancement through preserving dynamic security is worthy of study which is not covered in the available literature, yet. Such an approach deems vital since in case of dynamic insecurity and losing DERs, black starting under severe weather conditions would be very difficult. To fill this gap, an adaptive emergency approach is presented in this paper which aims at expediting the resilient operation of hybrid NμGs. The main contributions of this paper are:

- Developing an analytical method, which is based on region of attraction concept in non-linear control theory, to identify the dynamic security boundaries of a hybrid NμGs.
- Proposing a suite of emergency approaches to maintain the DERs in-service before reaching the boundaries of dynamic insecurity. The proposed emergency countermeasures adapt to different operation conditions of the hybrid NμGs.
- Embedding hazard characteristic in countermeasures identification process;
- Exploiting the potential of NμGs facilities to prevent the need for black-start and mitigate impacts of extreme events.

II. PROPOSED METHODOLOGY

A. OVERVIEW

The chronological outline of the proposed adaptive emergency approach is depicted in Fig. 2. The main objective is to preserve the resilient operation of NμGs by preventing unnecessary tripping of the DERs after an unintentional islanding incident. To do so, a resilient operation zone (ROZ) is introduced and the operation trajectories of the NμGs are preserved within the ROZ through suite of emergency approaches. The ROZ is the locus of all points within state variables plan at which, the NμGs resilient operation is retrieved subsequent to an unintentional islanding incident. In the proposed method, unlike the conventional loss of mains protection schemes, DERs can remain in-service and enhance resilience of the hybrid NμGs as long as the DERs state variables lie within the boundaries of the ROZ. Only in case that the boundaries of the ROZ are violated, the corresponding DER is tripped to avoid likely damages.

In Fig. 2, Stage 1 deals with offline analysis to calculate the ROZ. In this regard, the dynamic security model is extracted first which describes the behavior of synchronous generator-based DERs (SGBDERs), inverter-based DERs (IBDERs), AC μGs, DC μGs, and hybrid NμGs while being subjected to unintentional islanding incident. The attained model is then used to calculate equilibrium points and the ROZ of the hybrid NμGs.

The ROZ calculated at Stage 1 is dependent on the operating point (loading level) of the NμGs which is handled at the Stage 2 of the proposed approach. At Stage 2, the

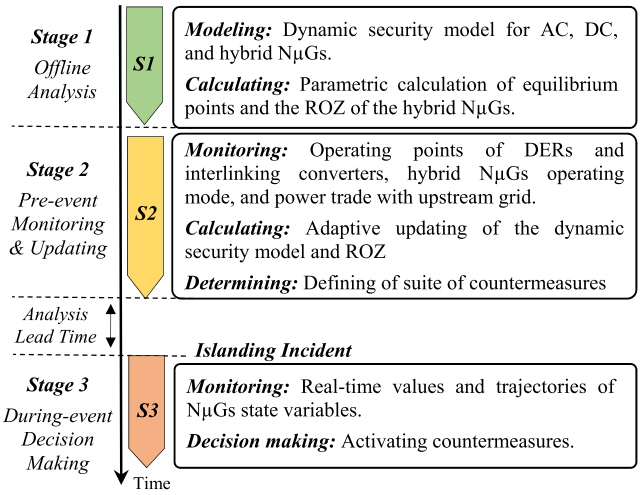

FIGURE 2. Proposed adaptive emergency approach for hybrid NμGs resilience.

NμGs equilibrium points and associated ROZ are updated in accordance with the operating point of hybrid NμGs. In other words, Stage 2 adapts the ROZ, which will be used at Stage 3, to the operation condition of hybrid NμGs. In addition, a suite of countermeasures, which will be used in the aftermath of the disaster, are determined in this stage. The analysis at Stage 2 is performed with a sufficient lead time for assurance purposes. After extreme event condition, the state variables of hybrid NμGs are monitored at Stage 3. The monitored values are compared with boundaries of the ROZ updated at Stage 2. Based on the performed comparison, the proper decisions are selected and implemented from the countermeasures determined at Stage 2.

B. MATHEMATICAL BACKGROUND

The terms and definitions utilized in this paper are discussed in this section. Afterwards, the proposed approach is presented in Sections II.C and II.D using these terms and definitions.

1) SGBDER DYNAMICS

Unintentional islanding from the main grid can be seen as a relatively large disturbance from the standpoint of small-scale SGBDERs in AC μGs. Hence, the equation of motion can be used to describe such condition [22], that is (in per-unit):

$$\begin{cases} \dot{\delta_s}^{\mu,ac} = \omega_0 . \Delta\omega_s^{\mu,ac} \\ \Delta\dot{\omega_s}^{\mu,ac} = (P_s^{m,\mu,ac} - P_s^{e,\mu,ac} - D_s^{\mu,ac}\Delta\omega_s^{\mu,ac}) \\ \qquad \times (2H_s^{\mu,ac})^{-1} \end{cases} \tag{1}$$

where,

$$\begin{aligned} P_s^{e,\mu,ac} = {} & (E_s^{\mu,ac})^2 Y_{ss}^{\mu,ac} \cos\theta_{ss}^{\mu,ac} \\ & + \sum_{\substack{b \in \mu B \\ b \neq s}} E_b^{\mu,ac} E_s^{\mu,ac} Y_{bs}^{\mu,ac} \\ & \times \cos(\delta_s^{\mu,ac} - \delta_b^{\mu,ac} - \theta_{bs}^{\mu,ac}) \end{aligned} \tag{2}$$

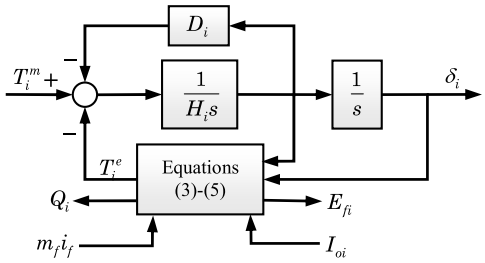

FIGURE 3. Block diagram of a synchronverter.

b, μB	Index and set of buses
s, μ, ac	Symbol of SGBDER, microgrid, AC microgrid
e, m	Symbol of electrical and mechanical quantities
D, H	Damping factor (p.u.), and inertia constant (second)
E	Voltage amplitude (p.u.)
P	Active power (p.u.)
$Y(\theta)$	Modulus (argument) of admittance matrix (p.u.)
ω_0	Nominal angular velocity (Rad./sec.)
δ, ω	Rotor angle (Rad.) and rotor angular velocity (Rad./sec.),
Δ, $\bullet$	Difference and derivative operators

2) IBDER DYNAMICS

The IBDERs controlled by the droop mechanism can be considered equivalent to a synchronverter [23], [24]. The synchronverter mimics the dynamics of a synchronous generator through the block diagram depicted in Fig. 3 and modeled by (3)-(5) [25]:

$$T_i^e = 1.5\, m_f i_f I_{oi} \cos(\delta_i - \varphi_i) \tag{3}$$

$$Q_i = 1.5\, m_f i_f I_{oi} \sin(\delta_i - \varphi_i) \tag{4}$$

$$E_i = \dot{\delta}_i\, m_f i_f \sin\delta_i \tag{5}$$

where,

i	Symbol of IBDER
$I_o(\varphi)$	Output current (angle) of IBDER (p.u.)
$m_f i_f$	Voltage set point of IBDER (p.u.)
Q, T	Reactive power (p.u.), torque (N.m)

Through the synchronverter model, the motion equation can represent the dynamics of IBDERs while being subjected to severe disturbances [7]:

$$\begin{cases} \dot{\delta_i}^{\mu,ac} = \omega_0 . \Delta\omega_i^{\mu,ac} \\ \Delta\dot{\omega_i}^{\mu,ac} = (P_i^{m,\mu,ac} - P_i^{e,\mu,ac} - D_i^{\mu,ac}\Delta\omega_i^{\mu,ac}) \\ \qquad \times (2H_i^{\mu,ac})^{-1} \end{cases} \tag{6}$$

where,

$$P_i^{e,\mu,ac} = 1.5\, E_{fi}^{\mu,ac} I_{oi}^{\mu,ac} \cos(\delta_i^{\mu,ac} - \varphi_i^{\mu,ac}) \tag{7}$$

where, E_f is the voltage set point of IBDER.

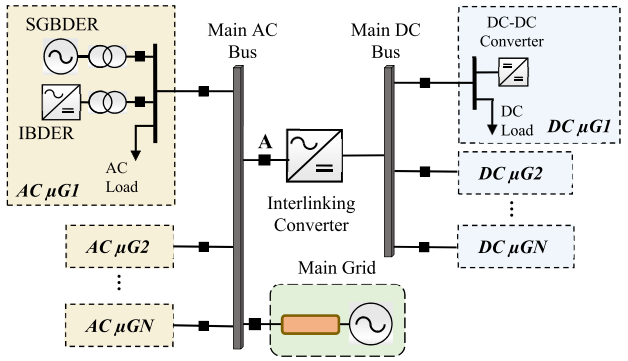

FIGURE 4. Hybrid AC/DC NμGs.

3) RESILIENT OPERATION ZONE (ROZ)

The ROZ is defined as the locus of all points at which, the NμGs resilient operation is retrieved when the disturbances imposed by the unintentional islanding incident are cleared. In other words, ROZ determines up to when it is secure to maintain the DERs in-service and stablish resilient operation. The properties of ROZ fit well with region of attraction concept in non-linear control theory [26] which is discussed in the following.

Consider a nonlinear system model as:

$$\dot{\mathbf{x}} = f(\mathbf{x}) \tag{8}$$

where, $\mathbf{x}$ us vector of state variables, f is a differentiable function from a domain $R_1 \subseteq R^n$ into R^n.

Definition 1: $\psi(t;\ \mathbf{x}_0)$ is the solution of (8), with an initial value of $\mathbf{x}(0) = \mathbf{x}_0$, evaluated at time $t \geq 0$. $\psi(t;\ \mathbf{x}_0)$ is the system trajectory which crosses $\mathbf{x}_0$.

Definition 2: A vector $\mathbf{x}^* \in R^n$ is an equilibrium point of (8) if $f(\mathbf{x}^*) = \mathbf{0}$. Here, * is superscript for equilibrium point.

Definition 3: The $\mathbf{x}^*$ associated with (8) is:

1) a stable equilibrium point if for any $\varepsilon \geq 0$, there exist a σ so that:

$$\left\|\mathbf{x}_0 - \mathbf{x}^*\right\| \leq \sigma \Rightarrow \left\|\psi(t;\ \mathbf{x}_0) - \mathbf{x}^*\right\| \leq \varepsilon \quad \forall t \geq 0; \tag{9}$$

where, ε, σ are small positive values and $\|\|$ is the norm operator.

2) an asymptotically stable equilibrium point if (9) and (10) are satisfied:

$$\left\|\mathbf{x}_0 - \mathbf{x}^*\right\| \leq \sigma \Rightarrow \lim_{t\to\infty} \psi(t;\ \mathbf{x}_0) = \mathbf{x}^* \tag{10}$$

3) an unstable equilibrium point if (9) does not hold.

Definition 4: The region of attraction associated with an asymptotically stable equilibrium point is:

$$\Re = \left\{\mathbf{x} \in R^n \middle|\ \lim_{t\to\infty}\ \psi(t;\ \mathbf{x}_0) = \mathbf{x}^*\right\} \tag{11}$$

$\Re$ is a set of points, such that any trajectory originating from $\mathbf{x}_0 \in \Re$ at time 0 will be attracted to the stable equilibrium point.

Theorem 1 (Lyapunov's indirect method) [27]: Let $\mathbf{A}$ be a Jacobian matrix of (8) at $\mathbf{x}^*$:

$$\mathbf{A} = \left.\frac{\partial f}{\partial \mathbf{x}}\right|_{\mathbf{x}=\mathbf{x}^*} \tag{12}$$

The $\mathbf{x}^*$ is an asymptotically stable equilibrium point of (8) if all the eigenvalues associated with $\mathbf{A}$ are located on the left-half plane which is denoted as secure equilibrium point (SEP), hereinafter. Likewise, $\mathbf{x}^*$ is unstable equilibrium point of (8) if $\mathbf{A}$ has eigenvalues on the right-half plane which is referred to as unsecure equilibrium points (UEPs), hereinafter.

C. STAGE 1: OFFLINE ANALYSIS

Given the hybrid AC/DC NμGs depicted in Fig. 4, this section represents the dynamics of a hybrid NμGs as the system denoted by (8).

The hybrid NμGs in Fig. 4 can be represented by the dynamics of associated center of inertia as:

$$\begin{cases} \dot{\delta_{CoI}}^{N\mu} = \omega_0.\,\Delta\omega_{CoI}^{N\mu} \\ \dot{\Delta\omega_{CoI}}^{N\mu} = (2H_{CoI}^{N\mu})^{-1}\left[P^{m,N\mu} - P^{e,N\mu} - D_{CoI}^{N\mu}\Delta\omega_{CoI}^{N\mu}\right] \end{cases} \tag{13}$$

where,

$$\delta_{CoI}^{N\mu} = (H_{CoI}^{N\mu})^{-1}\left[\sum_{\mu\in\Omega_{AC}} H_{CoI}^{\mu,ac}\delta_{CoI}^{\mu,ac} + H^{dc}\delta^{dc}\right] \tag{14}$$

$$\Delta\omega_{CoI}^{N\mu} = (H_{CoI}^{N\mu})^{-1}\left[\sum_{\mu\in\Omega_{AC}} H_{CoI}^{\mu,ac}\Delta\omega_{CoI}^{\mu,ac} + H^{dc}\Delta\omega^{dc}\right] \tag{15}$$

$$\begin{aligned} H_{CoI}^{N\mu} &= H^{dc} + \sum_{\mu\in\Omega_{AC}} H_{CoI}^{\mu,ac}, \\ D_{CoI}^{N\mu} &= D^{dc} + \sum_{\mu\in\Omega_{AC}} D_{CoI}^{\mu,ac} \end{aligned} \tag{16}$$

$$P^{m,N\mu} = P^{m,dc} + P^{m,ac}, \quad P^{e,N\mu} = P^{e,dc} + P^{e,ac} \tag{17}$$

where, *CoI* is the subscripts for buses and center-of-inertia, Ω_{AC} is set of AC μGs, and *dc* and $N\mu$ are symbols of DC microgrids and networked microgrids, respectively. In (14) and (15), $\delta_{CoI}^{\mu,ac}$ and $\Delta\omega_{CoI}^{\mu,ac}$ are rotor angle and rotor angular velocity associated with center of inertia of each AC μG calculated as:

$$\begin{aligned} \delta_{CoI}^{\mu,ac} &= \sum_{j\in DER\mu} \frac{H_j^{\mu,ac}\delta_j^{\mu,ac}}{H_{CoI}^{\mu,ac}}, \\ \Delta\omega_{CoI}^{\mu,ac} &= \sum_{j\in DER\mu} \frac{H_j^{\mu,ac}\Delta\omega_j^{\mu,ac}}{H_{CoI}^{\mu,ac}} \end{aligned} \tag{18}$$

where,

$$H_{CoI}^{\mu,ac} = \sum_{j\in DER\mu} H_j^{\mu,ac}, \quad D_{CoI}^{\mu,ac} = \sum_{j\in DER\mu} D_j^{\mu,ac} \tag{19}$$

and $DER\mu$ is set of DERs within the $\mu^{th}\mu$G. In (18), $DER\mu$ set includes both SGBDERs and IBDERs within the μ^{th} AC μG. Here if j^{th} DER is a SGBDER, $\delta_j^{\mu,ac}$ and $\Delta\omega_j^{\mu,ac}$ follow the dynamics expressed by (1); otherwise, (6) represent the dynamics of $\delta_j^{\mu,ac}$ and $\Delta\omega_j^{\mu,ac}$. Note that the batteries are usually connected to the AC systems through an inverter. In case the inverter of the battery is operated as the grid forming DERs within an AC μG, the dynamics can also be represented by (6). In case the batteries are operation in grid following mode, they can contribute to the countermeasures by rapidly charging and discharging which is discussed in Table 2.

The DC μGs in Fig. 4 are connected to the AC bus through an interlinking converter. In other words, the DC NμGs are seen as a large IBDER from AC bus standpoint with the rating equal to sum of DERs rating connected to the DC bus. Hence, δ^{dc} and $\Delta\omega^{dc}$ in (14) and (15) follow the dynamics represented in (6). In (14)-(16), H^{dc} and D^{dc} are:

$$\begin{aligned} H^{dc} &= \sum_{\mu\in\Omega_{DC}}\sum_{i\in DER\mu} H_i^{\mu,dc}, \\ D^{dc} &= \sum_{\mu\in\Omega_{DC}}\sum_{i\in DER\mu} D_i^{\mu,dc} \end{aligned} \tag{20}$$

where, Ω_{DC} is set of DC μGs. In (17), $P^{m,N\mu}$ represents the total input power to the DERs within a NμGs. This can be mechanical power for SGBDERs and DC power to the IBDERs. The electrical and mechanical (input) quantities in (17) are calculated as:

$$\begin{aligned} P^{m,dc} &= \sum_{\mu\in\Omega_{DC}}\sum_{i\in DER\mu} P_i^{m,\mu,dc}, \\ P^{m,ac} &= \sum_{\mu\in\Omega_{AC}}\sum_{j\in DER\mu} P_j^{m,\mu,ac} \end{aligned} \tag{21}$$

$$P^{e,dc} = \sum_{\mu\in\Omega_{DC}}\sum_{i\in DER\mu} 1.5E_{fi}^{\mu,dc}I_{oi}^{\mu,dc}\cos(\delta_i^{\mu,dc}-\varphi_i^{\mu,dc}) \tag{22}$$

$$P^{e,ac} = \sum_{\mu\in\Omega_{AC}}\sum_{j\in DER\mu} P_j^{e,\mu,ac} \tag{23}$$

Once the dynamic model of the hybrid NμGs is devised in the form of (8), the ROZ can be calculated using *Definition 4* in Section II.B.3, (11). The first step is to calculate the SEPs and UEPs which is performed by applying *Definition 2* in Section II.B.3 to (13). The equilibrium points of the hybrid NμGs represented by (13) are:

$$\mathbf{x}_{CoI}^{N\mu\ (1)(2)*} = \frac{\sum_{\mu\in\Omega_{DC}}\sum_{i\in DER\mu} H_i^{\mu,dc}\mathbf{x}_i^{dc(1)(2)*} + \sum_{\mu\in\Omega_{AC}} H_{CoI}^{\mu,ac}\mathbf{x}_{CoI}^{\mu,ac(1)(2)*}}{H_{CoI}^{N\mu}} \tag{24}$$

where,

$$\mathbf{x}_i^{dc(1),(2)*}: \quad \delta_i^{dc(1),(2)*} = \varphi_i^{\mu.dc} \mp \cos^{-1}\frac{P_i^{m,\mu.dc}}{1.5\,E_{fi}^{\mu.dc}I_{oi}^{\mu.dc}},$$

$$\Delta\omega_i^{dc(1)*} = 0 \tag{25}$$

$$\mathbf{x}_{CoI}^{\mu,ac(1)(2)*} = \sum_{j\in DER\mu}(H_{CoI}^{\mu,ac})^{-1}H_j^{\mu,ac}\mathbf{x}_j^{\mu,ac(1)(2)*} \tag{26}$$

In (25), the negative sign corresponds to $\mathbf{x}_i^{dc(1)*}$ and positive sign stands for $\mathbf{x}_i^{dc(2)*}$. In (26), the index j encompasses both SGBDERs and IBDERs with in an AC μG. The discriminated vectors of equilibrium points for SGBDERs and IBDERs are as (27) and (28), shown at the bottom of the next page.

In (27) and (28), the negative sign corresponds to $\mathbf{x}_s^{\mu,ac(1)*}$ and $\mathbf{x}_j^{\mu,ac(1)*}$; and, the positive is related to $\mathbf{x}_s^{\mu,ac(2)*}$ and $\mathbf{x}_i^{\mu,ac(2)*}$. The calculated equilibrium points, (25), (27), and (28) are evaluated by *Theorem 1* to identify associated security status. To do so, Jacobian matrix of (13) is formed by (29), shown at the bottom of the next page, and associated eigenvalues are calculated by solving (30), shown at the bottom of the next page, where, $\boldsymbol{\lambda}$ is matrix of eigenvalues.

In (30), the term $D_{CoI}^{N\mu}\Big/4H_{CoI}^{N\mu}$ is a positive value; hence, to have the left-half plane:

$$\frac{\partial P^{e,N\mu}}{\partial\delta_{CoI}^{N\mu}} > \left.\frac{\left(D_{CoI}^{N\mu}\right)^2}{8\omega_0 H_{CoI}^{N\mu}}\right|_{\mathbf{x}=\mathbf{x}_{CoI}^{N\mu(1)(2)*}} \tag{31}$$

The requirement in (31) is fulfilled when the δ_i^{dc*}, $\delta_s^{\mu,ac*}$, and $\delta_i^{\mu,ac*}$ in (25), (27) and (28) are less than $\pi/2$ radians. In (25), $\varphi_i^{\mu.dc}$ is close to $\pi/2$ radians since the IBDERs are usually connected to the microgrid through a relatively large coupling inductor. Hence, $\delta_i^{dc(1)*} \le \pi/2$ and $\delta_i^{dc(2)*} \ge \pi/2$. In (27), the $\delta_s^{\mu,ac*}$ is calculated based on (2) where, Y_{bs} elements are zero, except those representing the link between SGBDERs and the main AC bus, stated as $Y_{Ms}^{\mu.ac}$ in (27). The phase angle $\theta_{Ms}^{\mu.ac}$ associated with $Y_{Ms}^{\mu.ac}$ is close to $\pi/2$ radians representing high X/R ratio of SGBDERs and step-up transformers. Hence, $\delta_s^{\mu,ac(1)*}$ is less than and $\delta_s^{\mu,ac(2)*}$ is larger than $\pi/2$ radians. In (28), the condition is the same as (25) and $\delta_i^{\mu,ac(1)*}$ is less than $\pi/2$ radians. Therefore, based on the requirements stated by *Theorem 1* in Section II.B.3, $\mathbf{x}_{CoI}^{N\mu\ (1)*}$ and $\mathbf{x}_{CoI}^{N\mu\ (2)*}$are SEP and UEP, respectively.

Once the SEP and UEP are attained for hybrid NμGs, the region of attraction concept is calculated based on *Definition 4 in* Section II.B.3. The region of attraction associated with $\mathbf{x}_{CoI}^{N\mu\ (1)*}$ is an open and invariant set which is limited by the limit cycles of UEP, $\mathbf{x}_{CoI}^{N\mu\ (2)*}$. Here, the limit cycle is formed by calculating the system trajectory crossing $\mathbf{x}_{CoI}^{N\mu\ (2)*}$ [26]. Fig. 5 depicts the schematical representation of the secure and unsecure trajectories along with the limit cycle of $\mathbf{x}_{CoI}^{N\mu\ (2)*}$ for a hybrid NμGs demonstrated by (13). Here, the inner region of the limit cycle is the secure zone. In Fig. 5, the operating point of NμGs under normal operation conditions is $\mathbf{x}_{CoI}^{N\mu\ (1)*}$. By N$\mu$Gs islanding incident, the operating point of the NμGs moves from $\mathbf{x}_{CoI}^{N\mu\ (1)*}$ towards the boundaries of secure zone, i.e. the limit cycle in Fig. 5.

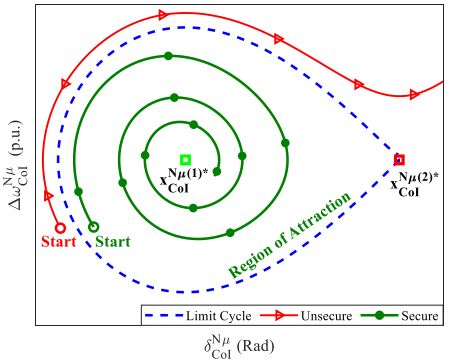

FIGURE 5. Secure and unsecure trajectories for hybrid NμGs.

Here, "Start" points indicate the locus of hybrid NμGs operating point at the time of remedial actions actuation. Referring to Fig. 5, if the remedial actions are actuated when the operating points is 'within the secure zone limits, the resilient operation of NμGs can be maintained (green Start point); otherwise, the situation yields in insecurity and all DERs within the NμGs should be tripped (red Start point).

D. STAGE 2: PRE-EVENT MONITORING & UPDATING

The outline of Stage 2 is depicted in Fig. 6. First step at Stage 2 is to monitor operating point of the NμGs, since the equilibrium points, associated region of attraction and consequently, ROZ is highly dependent on the operating point of the NμGs. The operational factors which are monitored at block #1 in Fig. 5 are NμGs operating mode (importing/exporting energy), power trade of the NμGs with upstream grid, transacted power of each μG with the rest of NμGs, and the operating point of the DERs. In addition, hazard condition is monitored to estimate the status of NμGs at post-islanding condition. Here, the hurricanes are taken into the account and the wind speed at pre-islanding stage is the main monitored factor. The pre-islanding data monitoring is repeated periodically with updating rate of T_{Update} seconds to adapt the emergency countermeasures to any change in NμGs operation condition (blocks #3 and #4). Note that, T_{Update} is directly dependent on the polling and updating rate of the NμGs data acquisition system and can be adjusted based on the characteristic of NμGs data acquisition system.

In block #5, a fragility analysis is performed which correlates the measured wind speed with the fragility curves of NμGs facilities using (32) [28]:

$$\text{Prob}_{Failure} = \int_0^{WS} \frac{e^{-0.5\times\left(SD^{-1}\ln\left(\frac{WS'}{Mean}\right)\right)^2}}{SD\times WS'\sqrt{2\pi}}\, dWS' \tag{32}$$

where, Mean and SD are mean and standard deviation values, WS is wind speed (m/s), and $Prob_{Failure}$ is the probability of failure. Here, the fragility of wind-based DERs and the main interconnecting links (MIL) which connect the μGs to the rest of the NμGs are taken in to the account. The main reason is that the failure in DERs would increase the power deficit originated from unintentional islanding and consequently, the amount of required remedial actions. On the other hand, failure in MIL would change the topology of NμGs and hence, the available facilities to stablish resilient operation of the NμGs.

The calculated failure probability in (32) is used to update the dynamic security model, (13), based on Table 1. The updated model augments performance of the proposed emergency approach by representing more realistic mimic of post-islanding condition. In Table 1, the failure for an asset is concluded in case the failure probability calculated in (32) is greater than a pre-defined value, say 70%. This value should be set by the NμGs operator through stablishing a

$$\mathbf{x}_s^{\mu,ac(1),(2)*}\begin{cases}\Delta\omega_s^{\mu,ac(1),(2)*}=0\\ \delta_s^{\mu,ac(1),(2)*}=\theta_{Ms}^{\mu,ac}\mp\cos^{-1}\dfrac{P_s^{m,\mu,ac}-\left(E_s^{\mu,ac}\right)^2 Y_{ss}^{\mu,ac}\cos\theta_{ss}^{\mu,ac}}{E_s^{\mu,ac}V_M Y_{Ms}^{\mu,ac}}\end{cases} \tag{27}$$

$$\mathbf{x}_i^{\mu,ac(1),(2)*}:\quad \delta_i^{\mu,ac(1),(2)*}=\varphi_i^{\mu,ac}\mp\cos^{-1}\frac{P_i^{m,\mu,ac}}{1.5\,E_{fi}^{\mu,ac}I_{oi}^{\mu,ac}},\qquad \Delta\omega_i^{\mu,ac(1)*}=0 \tag{28}$$

$$\mathbf{A}=\left[\begin{array}{cc}0 & \omega_0\\ -\frac{\partial P^{e,N\mu}}{\partial\delta_{CoI}^{N\mu}}(2H_{CoI}^{N\mu})^{-1} & -D_{CoI}^{N\mu}(2H_{CoI}^{N\mu})^{-1}\end{array}\right]_{\mathbf{x}=\mathbf{x}_{CoI}^{N\mu\ (1)(2)*}} \tag{29}$$

$$\begin{cases}\lambda^2+\dfrac{D_{CoI}^{N\mu}}{2H_{CoI}^{N\mu}}\lambda+\dfrac{\omega_0}{2H_{CoI}^{N\mu}}\dfrac{\partial P^{e,N\mu}}{\partial\delta_{CoI}^{N\mu}}=0\Big|_{\mathbf{x}=\mathbf{x}_{CoI}^{N\mu\ (1)(2)*}}\\ \lambda=-\dfrac{D_{CoI}^{N\mu}}{4H_{CoI}^{N\mu}}\pm\dfrac{1}{2}\sqrt{\left(\dfrac{D_{CoI}^{N\mu}}{2H_{CoI}^{N\mu}}\right)^2-\dfrac{2\omega_0}{H_{CoI}^{N\mu}}\dfrac{\partial P^{e,N\mu}}{\partial\delta_{CoI}^{N\mu}}}\Big|_{\mathbf{x}=\mathbf{x}_{CoI}^{N\mu\ (1)(2)*}}\end{cases} \tag{30}$$

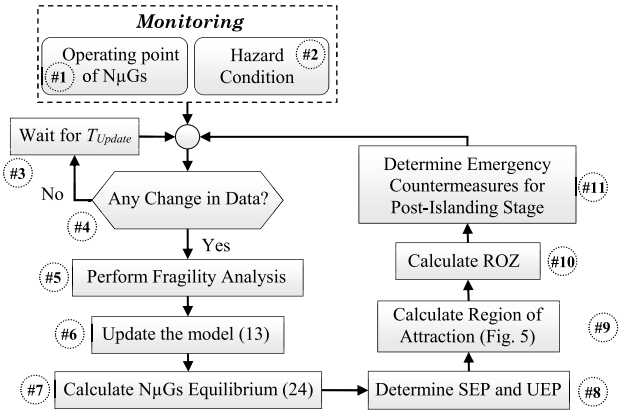

FIGURE 6. Outline of Stage 2 for the proposed emergency approach.

tradeoff between the resilience and amount of remedial action actuation.

The updated model in Block #6 is then used to calculate the equilibrium points using (24), determine associated security attribute, and calculate the region of attraction (blocks #7 to #9, respectively). Based on the region of attraction is calculated in Block #9 of Fig. 6, the ROZ is determined in Block #10. One may propose the utilization of the entire limit cycle as an index, in which the inside and the outside of limit cycle would be labeled as blocking and tripping zones, respectively. However, it could be demonstrated that portions of limit cycles, designated as the ROZ, is sufficient for developing the proposed resilience-oriented security measure. During grid-connected operation of NμGs, the total electrical power, i.e. $P^{e,N\mu}$ in (13), is equal to the $P^{m,N\mu}$ which is the sum of the power setpoint of IBDERs and mechanical input power of SGBDERs. On the other hand, $P^{e,N\mu}$ represents the net load of NμGs, i.e.

$$P^{e,N\mu}(t) = P^{N\mu}_{Load} - (1 - u(t-\tau))\, P^{e,N\mu}_{Trans} \tag{33}$$

where, *Trans* is subscript for transacted value and $u(t-\tau)$ expresses the step endured by $P^{e,N\mu}$ while being subjected to NμGs islanding incident. In Fig. 1, the $P^{e,N\mu}$ is roughly constant during the emergency dynamic security preservation stage; on the contrary, $P^{e,N\mu}$ follows the system dynamics. For emergency dynamic security preservation stage in Fig. 1, $\Delta\dot{\omega}^{N\mu}_{CoI}$ (13) can be expressed as:

$$\Delta\dot{\omega}^{N\mu}_{CoI} = r_1 - r_2 \Delta\omega^{N\mu}_{CoI} \tag{34}$$

where,

$$r_1 = (2H^{N\mu}_{CoI})^{-1}\left(P^{m,N\mu} - P^{e,N\mu}\right), \quad r_2 = (2H^{N\mu}_{CoI})^{-1} D^{N\mu}_{CoI} \tag{35}$$

Solving the differential equation represented by (34), and using $\Delta\omega^{N\mu}_{CoI} = \Delta\omega^{N\mu*}_{CoI}$ as the initial condition yields:

$$\Delta\omega^{N\mu}_{CoI} = r_1 r_2^{-1}(1 - e^{-r_2 t}) \quad \forall t \geq 0 \tag{36}$$

TABLE 1. Lookup table for model updating.

Failure		Considerations
DERs	MIL	
✓	✓	➢ Form (13) for NμGs excluding the μG which exposed to MIL failure. ➢ Update (13) by excluding the *H* and *D* of the failed DERs in (16). ➢ Add Generation amount of DER on top of the NμGs power transaction with the main grid at pre-islanding stage.
✓	×	➢ Update (13) by excluding the *H* and *D* of the failed DERs in (16). ➢ Add Generation amount of DER on top of the NμGs power transaction with the main grid at pre-islanding stage.
×	✓	➢ Form (13) for NμGs excluding the μG which exposed to MIL failure.
×	×	-

Here, $\delta^{N\mu}_{CoI}$ can be computed by placing (36) in (13) and solving the differential equation with $\delta^{N\mu}_{CoI} = \delta^{N\mu*}_{CoI}$ as the initial condition:

$$\delta^{N\mu}_{CoI} = r_1 r_2^{-1}\left(t + r_2^{-1} e^{-r_2 t} - r_2^{-1}\right) + \delta^{N\mu*}_{CoI} \quad \forall t \geq 0 \tag{37}$$

If the NμGs is importing power from the main grid at pre-event condition, r1 is a negative value. Referring to (36) and (37), for $r_1 \leq 0$, both $\Delta\omega^{N\mu}_{CoI}$ and $\delta^{N\mu}_{CoI}$ are monotonically decreasing within $\Delta\omega^{N\mu}_{CoI} \leq \Delta\omega^{N\mu*}_{CoI}$ and $\delta^{N\mu}_{CoI} \leq \delta^{N\mu*}_{CoI}$. In case of exporting power to the main grid, u2 is a positive value which yields both $\Delta\omega^{N\mu}_{CoI}$ and $\delta^{N\mu}_{CoI}$ to be monotonically increasing within $\Delta\omega^{N\mu}_{CoI} \geq \Delta\omega^{N\mu*}_{CoI}$ and $\delta^{N\mu}_{CoI} \geq \delta^{N\mu*}_{CoI}$. Therefore, the two portions of the limit cycle are sufficient to evaluate the hybrid NμGs security which are depicted in Fig. 7.

Block #11 in Fig. 6, determines the suite of countermeasure to be used after the unintentional islanding scenario is unfolded. The objective of these countermeasures is to alleviate the consequences of the disturbance before the time that trajectories pass the ROZ boundaries and tripping of all DERs has happen. Table 2 summarizes the countermeasures at Stage 2.

In case of exporting power to the main grid, the countermeasure with the priority is to charge the battery storage systems. In case of inadequacy, the next priority is prompt cutting down (not tripping) the outputs of IBDERs (including DERs at DC side) [29]. This can reduce the generation excess and maintain resilient operation without DER tripping. If the amount of IBDER curtailment is not sufficient, some SGBDERs might also be tripped as the second priority. The proposed method to determine sufficiency of a countermeasure for resilient operation is presented in Section II.E. In case of importing power from the grid, the priority is to rapidly discharge the battery storages. In case of insufficiency, the next priority is rapid load shedding is used where the load shedding priority will be defined by NμGs operator.

This stage monitors the state variables of the NμGs, i.e. $\delta^{N\mu}_{CoI}$ and $\Delta\omega^{N\mu}_{CoI}$, and maps the trajectory within the ROZ determined at Stage 2. Once the trajectory approaches the boundaries of the secure zone, the countermeasures defined

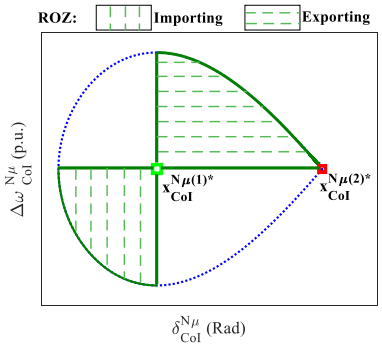

FIGURE 7. ROZ for hybrid NμGs operation.

TABLE 2. Lookup table for post-islanding condition estimation.

Operating mode	Remedial Action	Priority	Additional Considerations
Exporting power	DER Curtailment	1	Charging Battery Storages
		2	Reducing IBDERs Output
		3	Tripping SGBDERs
Importing power	Load Curtailment	1	Discharging Battery Storages
		2	Load shedding

by Table 1 at Stage 2 will be realized. This is modeled as:

$$\Delta\omega^{N\mu}_{CoI} \leq \alpha \left| \Delta\omega_{LC}|_{\delta_{LC}=\delta^{N\mu}_{CoI}} \right| \tag{38}$$

where, $(\delta_{LC}, \Delta\omega_{LC})$ represents an ordered pair corresponding to the limit cycle (boundaries of the secure zone). $0 \leq \alpha \leq 1$ determines the time for the countermeasures actuation. Here, $\alpha = 1$ represents the ROZ in Fig. 8 which corresponds to the theoretical threshold. By reducing α, the resilience operation zone diminishes which allows us to consider a safety margin to compensate practical inaccuracies (e.g. delays in communications, measurement errors, etc.). With respect to the practical considerations, large value for α may result in late actuation of the countermeasures which endangers the resilience of NμGs. On the contrary, small α values may increase the sensitivity of the proposed ROZ-based approach to the transients and the countermeasures might be unnecessarily actuated for small disturbances. Therefore, a trade-off by should be established in determining the α value in a way that neither the security nor the dependability of the proposed scheme will be jeopardized. In the proposed approach, α is considered as the setting which should be set by the NμGs operator\decision maker.

The required amount of countermeasures to be applied at the post-islanding stage is equal to the amount of NμGs power transaction with the main grid at pre-islanding stage (assuming that load conditions have not changed from pre- to post-event stages). The countermeasures are actuated by violating the brown dashed line in Fig. 8.

The load curtailment-based countermeasures can be directly applied. However, for DER curtailment-based countermeasure, the curtailment occurs through the logic depicted in Fig. 9 which combines local decision with NμG-wide decision:

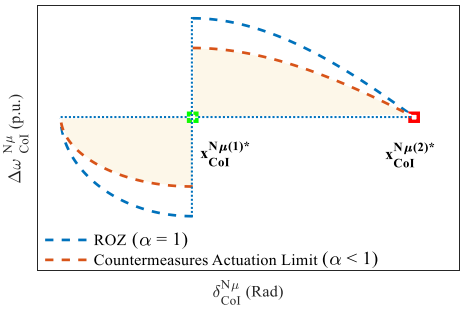

FIGURE 8. Steps of countermeasures actuation.

III. SIMULATION RESULTS

This section examines the proposed scheme on a system depicted in Fig. 10.

The system data are available in [4] where μGs1 and 2 are considered as the AC and the rest are DC μGs. The DER installed capacity and the peak load associated with each are reported in Table 3. The studied cases are represented in Table 4. Here, the α in (38) is considered 0.7 which is determined based on the dynamics of the hybrid NμGs under study and simulation studies. The updating rate of NμGs with data acquisition system is assumed to be 1 second. Hence, T_{Update} in Fig. 6 is considered to be 1 second. In this study, the simulations are conducted using the DIgSILENT Power Factory software in a personal computer with Intel Core^{TM}i7 CPU @3 GHz and 12 GB RAM.

The simulation results for Cases I and II in Table 4 are presented in Figs. 11 and 12. At pre-islanding stage, the NμGs is operation point on associated SEP; hence, the locus of NμGs state variables is on the $\mathbf{x}^{N\mu\ (1)*}_{CoI}$ in Fig. 11. Here, the time required to form ROZ at pre-islanding stage is 600 ms and 400 ms for Cases I and II, respectively. Following to an islanding incident, the state variables move toward the boundaries of ROZ within $\Delta\omega^{N\mu}_{CoI} \leq \Delta\omega^{N\mu*}_{CoI}$ and $\delta^{N\mu}_{CoI} \leq \delta^{N\mu*}_{CoI}$ region for Case I (Fig. 11(a)) and within $\Delta\omega^{N\mu}_{CoI} \geq \Delta\omega^{N\mu*}_{CoI}$ and $\delta^{N\mu}_{CoI} \geq \delta^{N\mu*}_{CoI}$ region for Case II (Fig. 11(b)). This observation is in line with the discussion made in Fig. 7.

In Case I, the pre-islanding energy trade between NμGs and the main grid is 5.2 MW (import). Referring to Fig. 11(a), in case the 5.2 MW load is curtailed at T1, which the time NμGs trajectories exceed the boundaries of countermeasures actuation limit, the NμGs trajectories are steered towards the SEP and resilient operation of NμGs can be retrieved. This can also be observed from temporal characteristic of rotor angular velocity at NμGs center of inertia in Fig. 12(a). On the contrary, resilient operation of NμGs is forfeited when the 5.2 MW load curtailment is occurred at T2 in Fig. 11(b), i.e. beyond the ROZ. Here, the pole slip event in Fig. 12(b) yields in insecurity which in turn, results in tripping of all DERs and losing 10 MW load.

In Case II, 4.45 MW was exporting at pre-islanding stage where corresponding countermeasure to maintain NμGs resilience is 4.45 MW DER curtailment. In Fig. 11(b), the resilient operation of the NμGs is preserved by curtailing

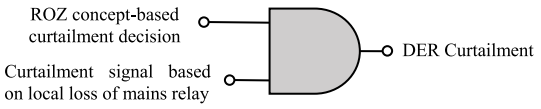

FIGURE 9. Logic of DER curtailment (in case needed) subsequent to unintentional islanding event.

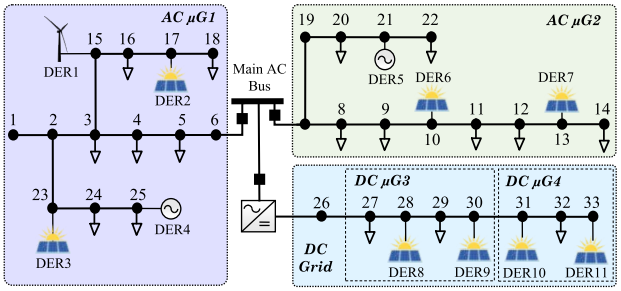

FIGURE 10. 33-bus distribution system composed of four interconnected μGs operating as hybrid NμGs [4].

TABLE 3. DERs and peal load at each μG.

	AC μG1	AC μG2	DC μGs
Installed DER Capacity	DER1= 0.8 MW DER2= 0.5 MW DER3= 0.5 MW DER4= 3 MW	DER5 = 2 MW DER6= 0.5 MW DER7= 0.5 MW	DER8 = 1 MW DER9 = 1 MW DER10 = 1 MW DER11 = 1 MW
Peak Load	10 MW	8 MW	4 MW
Min Load	1 MW	1 MW	0.5 MW

TABLE 4. Cases under study.

Case	AC μG1 (MW)		AC μG2 (MW)		DC NμGs (MW)		Power Transaction
	Gen.	Load	Gen.	Load	Gen.	Load	
I	3	2	1.8	7	0	1	5.2 MW Import
II	3	1.8	1.8	1	3.45	1	4.45 MW Export

4.45 MW DER curtailment at T3, where the NμGs trajectories violate the boundaries of countermeasures actuation limit. Doing so, the resilient operation of NμGs is provided and 3.8 MW load is served at post-islanding stage. However, if 4.45 MW is curtailed outside the ROZ, i.e. T4 in Fig. 11(b), the resultant situation yields in insecurity. The insecurity is emerged as the pole slip incident in Fig. 12(d) which brings about tripping of all DERs and losing 3.8 MW load. As can be seen, by the proposed ROZ-based approach in place, the resilient operation of the NμGs subsequent to an unintentional event is maintained at both Cases I and II. Referring to Fig. 12, both Cases I and II are settled down roughly 15 second after the islanding incident by actuating the remedial actions within ROZ limits; however, such settlements require emergency actions during dynamic security preservation stage (see Fig. 1). The main reason is low inertia of hybrid NμGs which results in fast transients. Comparing Fig. 12(a) and (b), if the remedial action in T1 is applied 150 ms later, that is T2, the resilient operation can not be maintained. Based on these observations, it can be concluded that the proposed ROZ is an effective tool to discriminate the secure operating zone of the NμGs and the limits for implementing the corrective countermeasures.

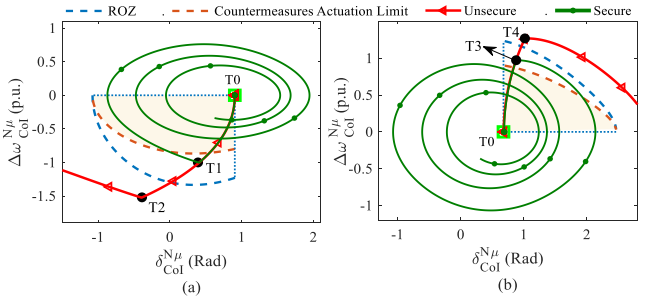

FIGURE 11. Trajectories of NμGs for: a) Case I; b) Case II.

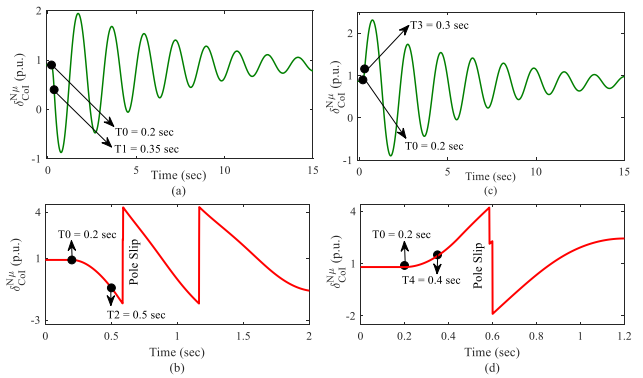

FIGURE 12. Temporal characteristic for rotor angular velocity at NμGs center of inertia: a) Case I – load shedding at T1; b) Case I – load shedding at T2; c) Case II – DER curtailment at T3; d) Case II – DER curtailment at T4.

To validate the proposed method adaptability, the simulation results for different cases are reported in Table 5 are presented in Table 6. Here, the performance of the proposed scheme (PS) is compared with out-of-step (OOS) relay-based [13] and undervoltage (UV) relay-based [14] approaches as the common loss of mains practices. The settings of OOS relay is derived from [30], i.e. DER tripping after one pole slip incident. For UV relay, the settings are 0.8 p.u. with 200 ms delay as recommended by [13]. Note that, the main objective of the proposed method is maintaining the resilience through supply continuity. Hence, the main index used in Table 6 for comparison is the amount of load which curtailed/rescued after unintentional islanding incident.

In Table 6, PS rescued considerable amount of load in all listed cases. In cases where the NμGs is importing power from the main grid, i.e. Cases I, III, IV, IX, and X, the immediate tripping of DERs through the local loss of mains relays are avoided and DERs are maintained in service through the logic depicted in Fig. 9. Doing so, the considerable amount of load, which is equal to the in-service on-site DERs, is rescued. In cases where the NμGs is exporting power to the main grid, i.e. Cases II, V, and VI, 100% of the load is rescued upon unintentional islanding. The main reason is availability of sufficient on-site DERs which are kept in-service through the proposed approach and contributed to resilient operation. The results outlined in Table 4 demonstrate that PS is capable of adapting to different operation condition of NμGs. Unlike the PS, the deployment of OOS and UV schemes in most cases resulted in substantial load curtailment.

TABLE 5. Cases under study.

Case	Generation (MW)			Load (MW)	Scenario
	PV	Wind	Diesel		
I	1.2	0.8	2.8	10.0	Typical import
II	4.65	0.8	2.8	3.8	Typical export
III	6	0.8	3.0	22.0	Max. load, max local generation
IV	6	0.8	0.0	22.0	Max. load, only renewable generation
V	6	0.8	3.0	2.5	Min load, max local generation
VI	6	0.8	0.0	2.5	Min load, only renewable generation
VII	6	0.8	3.0	9.8	No exchange, low reactive power exchange
VIII	2.1	0.4	0.0	2.5	No exchange, high reactive power exchange
IX	0	0.8	1.5	8.8	Islanding at night, no solar generation
X	3	0.8	1.5	10.0	Islanding at extreme wind

TABLE 6. Simulation results for different cases.

Case	Exchange (MW)	Load Curtailment (MW)			Rescued Load (%)		
		PS[1]	OOS[2]	UV[3]	PS	OOS	UV
I	5.2 (Import)	5.2	10	10	48%	0%	0%
II	4.45 (Export)	0	3.8	3.8	100%	0%	0%
III	12.2 (Import)	12.2	22	22	44.5%	0%	0%
IV	15.2 (Import)	15.2	22	22	30%	0%	0%
V	7.3 (Export)	0	2.5	2.5	100%	0%	0%
VI	4.3 (Export)	0	2.5	2.5	100%	0%	0%
VII	0	0	0	0	100%	100%	100%
VIII	0	0	0	0	100%	100%	0%
IX	6.5 (Import)	6.5	8.8	8.8	26%	0%	0%
X	4.7 (Import)	5.5	10	10	45%	0%	0%

[1]PS: Proposed Scheme
[2]OOS: Out-Of-Step relay-based approach
[3]UV: Undervoltage relay-based approach

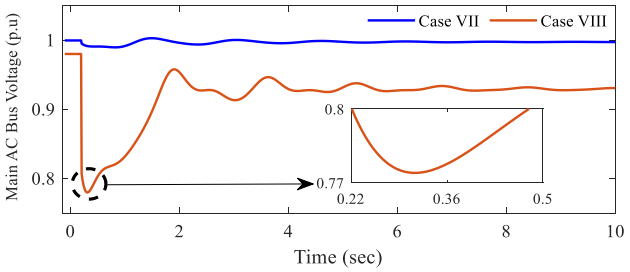

FIGURE 13. Temporal characteristic for voltage at main AC bus.

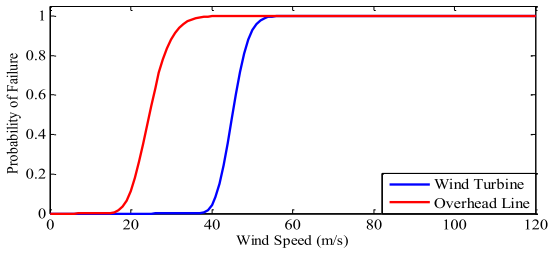

FIGURE 14. Fragility curves for wind turbines and overhead lines.

In Case VII, where no active power and low reactive power, i.e. 100 kVAr, exchange with the main grid is envisioned, deployment of OOS and UV schemes contributed to no load curtailment. However, when high reactive power exchange is required (6 MVAr), 100% of the load is curtailed by UV. The main reason is the drastic voltage drop which occurs after unintentional islanding at Case VIII (see Fig. 13). In Fig. 13, the voltage amplitude is less than 0.8 p.u. for more than 200 ms which renders UV scheme to trip the DERs. However, even under such a condition, the PS can rescue the loads and boost up resilience of the NμGs. The simulation results in

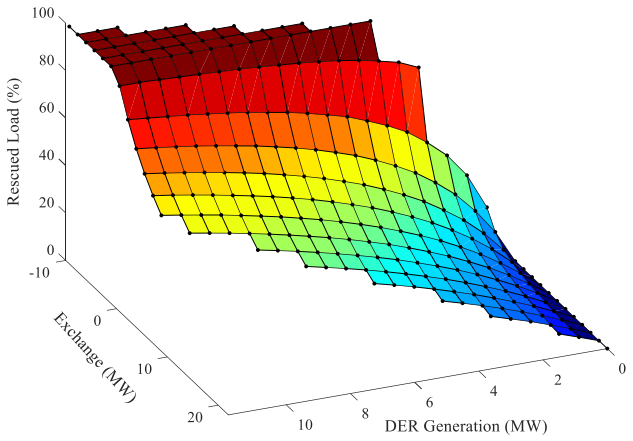

FIGURE 15. Rescued load after unintentional islanding for different DER generation and exchange with main grid conditions.

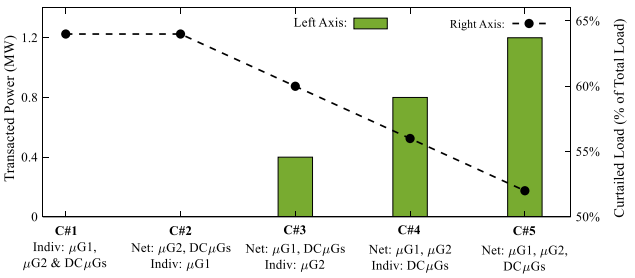

FIGURE 16. Rescued load after unintentional islanding for different network structure.

Table 6 implies the undesirable impact of the available loss of mains protection schemes on the resilience of the NμGs.

Case X in Table 5 expresses a scenario where unintentional islanding is occurred at extreme wind condition. For this case, the wind speed is given 50 m/s. The fragility curves for wind-based DERs and overhead lines connecting buses 6, 7 and DC NμGs to the main AC bus are depicted in Fig. 14 [28]. Referring to Fig. 14, 50 m/s wind speed results in failure of DER1 in AC μG1 and also splitting of NμGs from each other due to failure of main interconnecting links. Here unlike other cases, the load curtailment by the PS is 5.5 MW which is more than NμGs power transaction with the main grid at pre-islanding stage, 4.7 MW. The main reason is that according to Table 1, the generation of DER1 (0.8 MW) is added on top of the NμGs power transaction with the main grid at pre-islanding stage.

Fig. 15 depicts the rescued load after unintentional islanding for different DER generation and exchange with main grid conditions. In Fig. 15, negative values for exchange represent the export to the main grid where, the resilient operation of the NμGs is fully attained and all loads within the NμGs is rescued.

The amount of rescued load decreases as the DER generation decreases which confirm the direct impact of on-site DERs on the resilience of power system. When the exchange with the main grid turns into positive values, the amount of rescued load decreases. The reason is that the positive

exchange values account for import from the main grid mode that is equivalent to excess of load from the on-site DER generation. This observation reveals the necessity of adopting an adaptive approach, such as PS, to maintain the resilient operation of NμGs.

Fig. 16 represent the performance of the PS in Case I of Table 6 for different network configurations. Here, five configurations are considered for NμGs depicted in Fig. 10. As can be seen, the PS can improve power system resilience even if the μGs are not networked. However in Fig. 16, the amount of load curtailment is reduced as we increased the connectivity among the μGs which in turn, increases the transacted power among the μGs. This observation expresses effectiveness of the NμGs for augmenting power system resilience and reducing the damaging impacts of electricity interruptions.

IV. CONCLUSION

This paper dealt with augmentation of NμGs resilience through maintaining dynamic security. Here, a three-stage emergency approach was proposed which aims at preserving the resilient operation of NμGs by preventing unnecessary tripping of the DERs after unintentional islanding incident. A resilient operation zone (ROZ) was introduced and the operation trajectories of the NμGs are preserved within the ROZ through suite of emergency approaches. The conducted studies in this paper concluded that: 1) The available loss of mains protection schemes could jeopardize the resilient operation of the NμGs; 2) By adopting suite of proper countermeasures, such as the proposed approach, the negative impact of loss of mains protection schemes on resilient operation of NμGs can be compensated for; 3) The proposed ROZ is an effective tool to discriminate the secure operating zone of the NμGs and the limits for implementing the corrective countermeasures for resilience augmentation; 4) The amount of rescued load subsequent to an unintentional islanding event is highly dependent on the operation point of NμGs at pre-islanding stage which is tackled through adaptive feature of the proposed approach; 5) The proposed approach can improve the resilience even if the μGs are not networked; however, networking μGs and stablishing NμGs adds to the effectiveness of the proposed approach in further improvement of power system resilience.

Regarding the limitations of the proposed approach, it is worth mentioning that the proposed approach relies on the estimation of ROZ. The precision of estimated ROZ may depend on the accuracy of NμGs dynamic security model (13). For the presented NμGs it is shown that the approximated dynamic security model is sufficiently accurate (see figure 11). In case of application of the proposed method to a more complex NμGs, accuracy of the dynamic security model of the NμGs must be carefully verified. The other limitation might be deployment of fragility curve for estimating the post-islanding condition which imposes probability-based decision making for post-islanding conditions. Although the proposed approach is still applicable, the uncertainties originated from probability-based decision making may reduce the precision level of decision making for the countermeasures.

Future works may consider the scalability issues regarding the type and the number of components of the NμGs and communication standpoints. In particular, the effect of electrical vehicle, for instance vehicle to grid model, could be investigated. Furthermore, the performance of the proposed approach in real-world applications could be studied through experimental investigation. To this end, the authors aimed at performing experimental validation tests in the reconfigurable distribution grid laboratory of HEIG-VD, in Yverdon-les-Bains, Switzerland [31].

REFERENCES

[1] X. Liu, M. Shahidehpour, Z. Li, X. Liu, Y. Cao, and Z. Bie, "Microgrids for enhancing the power grid resilience in extreme conditions," *IEEE Trans. Smart Grid*, vol. 8, no. 2, pp. 589–597, Mar. 2017.

[2] S. Teimourzadeh, O. B. Tor, M. E. Cebeci, A. Bara, and S. V. Oprea, "A three-stage approach for resilience-constrained scheduling of networked microgrids," *J. Modern Power Syst. Clean Energy*, vol. 7, no. 4, pp. 705–715, Jul. 2019.

[3] Z. Li, M. Shahidehpour, F. Aminifar, A. Alabdulwahab, and Y. Al-Turki, "Networked microgrids for enhancing the power system resilience," *Proc. IEEE*, vol. 105, no. 7, pp. 1289–1310, Jul. 2017.

[4] L. Che and M. Shahidehpour, "DC microgrids: Economic operation and enhancement of resilience by hierarchical control," *IEEE Trans. Smart Grid*, vol. 5, no. 5, pp. 2517–2526, Sep. 2014.

[5] A. Shaker, A. Safari, and M. Shahidehpour, "Reactive power management for networked microgrid resilience in extreme conditions," *IEEE Trans. Smart Grid*, vol. 12, no. 5, pp. 3940–3953, Sep. 2021.

[6] Z. Ye, C. Chen, B. Chen, and K. Wu, "Resilient service restoration for unbalanced distribution systems with distributed energy resources by leveraging mobile generators," *IEEE Trans. Ind. Informat.*, vol. 17, no. 2, pp. 1386–1396, Feb. 2020.

[7] S. Teimourzadeh, F. Aminifar, M. Davarpanah, and M. Shahidehpour, "Adaptive protection for preserving microgrid security," *IEEE Trans. Smart Grid*, vol. 10, no. 1, pp. 592–600, Jan. 2019.

[8] *IEEE Standard for Interconnecting Distributed Resources With Electric Power Systems*, IEEE Standard 1547-2003, 2003, pp. 1–28.

[9] F. Iov, A. D. Hansen, P. E. Sorensen, and N. A. Cutululis, "Mapping of grid faults and grid codes," Riso Nat. Lab., Tech. Univ. Denmark, Roskilde, Denmark, Tech. Rep. Risø-R-1617, 2007.

[10] L. Zhang, C. Wang, J. Liang, M. Wu, B. Zhang, and W. Tang, "A coordinated restoration method of hybrid AC/DC distribution network for resilience enhancement," *IEEE Trans. Smart Grid*, early access, Jul. 21, 2022, doi: 10.1109/TSG.2022.3192910.

[11] S. Teimourzadeh, F. Aminifar, M. Davarpanah, and M. Shahidehpour, "Adaptive control of microgrid security," *IEEE Trans. Smart Grid*, vol. 9, no. 4, pp. 3909–3910, Jul. 2018.

[12] K. Malmedal, P. K. Sen, and J. P. Nelson, "Application of out-of-step relaying for small generators in distributed generation," *IEEE Trans. Ind. Appl.*, vol. 41, no. 6, pp. 1506–1514, Nov. 2005.

[13] S. Teimourzadeh, F. Aminifar, and M. Davarpanah, "Microgrid dynamic security: Challenges, solutions and key considerations," *Electr. J.*, vol. 30, no. 4, pp. 43–51, May 2017.

[14] E. J. Coster, J. M. A. Myrzik, and W. L. Kling, "Influence of protection on transient stability of medium voltage grids including distributed generation," in *Proc. 42nd Int. Universities Power Eng. Conf.*, Sep. 2007, pp. 1054–1059.

[15] R. Razzaghi, M. Davarpanah, and M. Sanaye-Pasand, "A novel protective scheme to protect small-scale synchronous generators against transient instability," *IEEE Trans. Ind. Electron.*, vol. 60, no. 4, pp. 1659–1667, Apr. 2013.

[16] Y. Zhang, Q. Sun, J. Zhou, L. Li, P. Wang, and J. M. Guerrero, "Coordinated control of networked AC/DC microgrids with adaptive virtual inertia and governor-gain for stability enhancement," *IEEE Trans. Energy Convers.*, vol. 36, no. 1, pp. 95–110, Mar. 2021.

[17] Q. Hui, J. Yang, X. Yang, Z. Chen, Y. Li, and Y. Teng, "A robust control strategy to improve transient stability for AC–DC interconnected power system with wind farms," *CSEE J. Power Energy Syst.*, vol. 5, no. 2, pp. 259–265, Jun. 2019.
[18] X. Li, Z. Li, L. Guo, J. Zhu, Y. Wang, and C. Wang, "Enhanced dynamic stability control for low-inertia hybrid AC/DC microgrid with distributed energy storage systems," *IEEE Access*, vol. 7, pp. 91234–91242, 2019.
[19] Q. Zhou, M. Shahidehpour, A. Alabdulwahab, and A. Abusorrah, "Flexible division and unification control strategies for resilience enhancement in networked microgrids," *IEEE Trans. Power Syst.*, vol. 35, no. 1, pp. 474–486, Jan. 2020.
[20] L. He, Y. Li, J. M. Guerrero, and Y. Cao, "A comprehensive inertial control strategy for hybrid AC/DC microgrid with distributed generations," *IEEE Trans. Smart Grid*, vol. 11, no. 2, pp. 1737–1747, Mar. 2020.
[21] Y. Du, X. Lu, B. Chen, and F. Lin, "Resiliency augmented hybrid AC and DC distribution systems with inverter-dominated dynamic microgrids," *IEEE Trans. Smart Grid*, vol. 13, no. 5, pp. 4088–4101, Sep. 2022.
[22] P. Kundur, N. J. Balu, and M. G. Lauby, *Power System Stability and Control*. New York, NY, USA: McGraw-Hill, 1994.
[23] J. Rocabert, A. Luna, F. Blaabjerg, and P. Rodriguez, "Control of power converters in AC microgrids," *IEEE Trans. Power Electron.*, vol. 27, no. 11, pp. 4734–4749, Nov. 2012.
[24] S. D'Arco and J. A. Suul, "Equivalence of virtual synchronous machines and frequency-droops for converter-based microgrids," *IEEE Trans. Smart Grid*, vol. 5, no. 1, pp. 394–395, Jan. 2014.
[25] Q.-C. Zhong and G. Weiss, "Synchronverters: Inverters that mimic synchronous generators," *IEEE Trans. Ind. Electron.*, vol. 58, no. 4, pp. 1259–1267, Apr. 2011.
[26] H. Khalil, *Nonlinear Systems*. New York, NJ, USA: Prentice-Hall, 2002.
[27] S. H. Zak, *Systems and Control*. New York, NY, USA: Oxford Univ. Press, 2003.
[28] R. Mo, H. Kang, M. Li, and X. Zhao, "Seismic fragility analysis of monopile offshore wind turbines under different operational conditions," *Energies*, vol. 10, no. 7, p. 1037, Jul. 2017.
[29] Y. Huang, G. Li, C. Chen, Y. Bian, T. Qian, and Z. Bie, "Resilient distribution networks by microgrid formation using deep reinforcement learning," *IEEE Trans. Smart Grid*, early access, Jun. 1, 2022, doi: 10.1109/TSG.2022.3179593.
[30] D. Reimert, *Protective Relaying for Power Generation Systems*. Boca Raton, FL, USA: CRC Press, 2005.
[31] M. Carpita, J.-F. Affolter, M. Bozorg, D. Houmard, and S. Wasterlain, "ReIne, a flexible laboratory for emulating and testing the distribution grid," in *Proc. 21st Eur. Conf. Power Electron. Appl. (EPE ECCE Eur.)*, Sep. 2019, pp. 1–6.

AYDA SHAKER (Student Member, IEEE) received the B.Sc. degree in electrical engineering and the M.Sc. degree (Hons.) in electrical engineering from the University of Tabriz, Iran, in 2016 and 2018, respectively. She is currently pursuing the Ph.D. degree with the School of Engineering, Azarbaijan Shahid Madani University, Tabriz, Iran. Since 2020, she has been collaborating with EPRA Electric Energy Company, Ankara, Turkey, as a Research and Development Researcher. She is also affiliated with the School of Management and Engineering Vaud (HEIG-VD), Institute of Energy and Electrical Systems (IESE), University of Applied Sciences and Arts of Western Switzerland (HES-SO), Yverdon-les-Bains, Switzerland, as an Exchange Ph.D. Research Scholar. Her research interests include power system operation, adaptive protection, microgrid resilience, and smart grid initiatives.

MOKHTAR BOZORG (Member, IEEE) received the B.Sc. and M.Sc. degrees in electrical engineering from the Sharif University of Technology, Tehran, Iran, in 2008 and 2011, respectively, and the Ph.D. degree from the Power System Research Group, Ecole Polytechnique Fédérale de Lausanne (EPFL), Lausanne, Switzerland, in 2015. From 2015 to 2018, he was a Postdoctoral Fellow and the Guest Scientist at the Distributed Electrical System Laboratory, EPFL. Since 2019, he has been an Associate Professor of energy and power systems with the School of Management and Engineering (HEIG-VD), Institute of Energy and Electrical Systems (IESE), University of Applied Sciences and Arts of Western Switzerland (HES-SO). His research interests include smart grids, active distribution networks, applications of mathematical modeling, optimization techniques, data analytics in power systems, integration of renewable energy sources, and energy storage systems into power systems.

AMIN SAFARI received the B.Sc. degree in electrical engineering from the University of Tabriz, Tabriz, Iran, in 2007, the M.Sc. degree from the University of Zanjan, in 2009, and the Ph.D. degree from the Iran University of Science and Technology, Tehran, Iran, in 2013. He is currently an Associate Professor with the Department of Electrical Engineering, Azarbaijan Shahid Madani University, Tabriz. His research interests include the application of artificial intelligence, heuristic optimization algorithms to power system design, FACTS, power system analysis and control, renewable energy, control and management of microgrids, and smart grid. In 2016, he was selected as a Distinguished Researcher at the Azarbaijan Shahid Madani University.

SAJAD NAJAFI-RAVADANEGH (Member, IEEE) received the Ph.D. degree in electrical engineering from the Department of Electrical Engineering, Amirkabir University of Technology (Tehran Polytechnic), Tehran, Iran, in 2009. He is currently a Professor with the Electrical Engineering Department, Azarbaijan Shahid Madani University, Tabriz, Iran, where he is responsible for the Resilient Smart Grids Research Laboratory.